JOURNAL OF GUIDANCE, CONTROL, AND DYNAMICS
Vol. , No. ,

Optimal Planar Powered Descent with Independent Thrust and Torque

Taylor P. Reynolds* and Mehran Mesbahi†
University of Washington, Seattle, Washington 98195

https://doi.org/10.2514/1.G004701

A powered descent problem with a body-fixed thrust vector and independent torque input is considered. By assuming that the entire descent maneuver takes place in an inertially-fixed plane, we show by using the maximum principle that the optimal thrust magnitude must lie on its boundary and may exhibit up to four switches with a min–max–min–max–min profile. The optimal torque input may be singular, and an expression for it is derived. Non-singular torque arcs are shown to be intimately related to the boundary conditions that are imposed on the vehicle's attitude and the presence of minimum thrust arcs at the beginning and end of the descent. Our results can be thought of as a generalization of previous work on three-degree-of-freedom translational powered descent; with new theoretical insights obtained for powered descent problems that consider attitude in the problem formulation.

I. Introduction

PROPELLANT-OPTIMAL powered descent refers to the problem of transferring a vehicle from some initial state to some target state by using rocket-powered engines and/or reaction control systems while expending the minimum amount of fuel. Research in the area of optimal powered descent began in earnest when the Apollo program set its sights on achieving a manned lunar landing. While Apollo guidance is not propellant-optimal, its designers were aware of theoretical results from early work that studied the problem of propellant-optimal powered descent [1–3]. Lawden derived several characteristics of optimal thrust programs for general three-degree-of-freedom (3-DOF) translational guidance trajectories, providing many key insights [2]. Subsequently, Ref. [4] provided numerical simulation results for the 3-DOF landing problem that built on Lawden's work using newly available software. Several authors have continued to look for analytical solutions to the first-order necessary conditions for the 3-DOF problem [5–9], and efficient numerical routines for obtaining optimal thrust programs (by solving the necessary conditions directly) have been developed [6,7].

Along similar lines, Açıkmeşe and Ploen have shown that these same analytic results from optimal control theory could be used to transform the (non-convex) 3-DOF problem into an equivalent convex optimal control problem [10]. This lossless convexification result bridged the gap between theoretical understanding of the 3-DOF guidance problem and the ability to guarantee the convergence of numerical routines by using convex optimization. The theory of lossless convexification has since been extended to include non-convex thrust pointing constraints [11–13] and minimum-landing error problems [14]. In addition, the numerical advantages of using convex optimization to solve the 3-DOF problem have been leveraged to develop viable flight software for planetary guidance missions [15–17].

Apollo guidance and each of the references heretofore provided are 3-DOF translational guidance methods for which attitude commands are (assumed to be) computed separately using a cascaded control architecture [1]. It is only recently that the generalized six-degree-of-freedom (6-DOF) guidance problem that considers both translational and rotational motion of a rigid body has been studied. A driving requirement behind this extension is the need to account for vision-based pointing constraints due to modern navigation sensors [18,19]. Such constraints couple the rotation and translation of the vehicle,‡ and cannot be easily enforced when the two are considered separately. Previous work on 6-DOF powered descent includes the use of model predictive control [20,21] and, more recently, feedforward trajectory generation techniques [22–26]. In contrast to the 3-DOF problem, however, each of these works provide numerical solution techniques to the 6-DOF landing problem; a characterization of the solution(s) to the necessary conditions of optimality for the propellant-optimal 6-DOF problem remains an open problem.

The primary contribution of this paper is the characterization of optimal solutions for a powered descent problem that lies between the 3-DOF and 6-DOF problems. This problem is referred to as a *planar landing problem* and has translational motion that is restricted to a plane with a single attitude variable. A similar problem was considered in [4], however, the authors used a simplified problem statement and as a result did not deduce the switching structure for the optimal thrust input that is proven in this work. By studying a slightly more general problem and employing different proof techniques, deeper insights are revealed and new conclusions are drawn. As a secondary contribution, the results given here can be used to verify the optimality of 6-DOF numerical algorithms that employ the same control configuration. By assuming that the vehicle's motion is restricted to a plane and that no state constraints are present (or at least are not active), the 6-DOF problem is equivalent to the planar landing scenario that is studied here. A suitably chosen set of problem parameters could therefore be used to assess optimality without having analytically solved the full 6-DOF problem.

This paper is organized as follows. The problem statement and notation are discussed in Sec. II, and the main results are presented in Sec. III. Section IV provides a numerical example that supports the key observations made in the preceding results section. Lastly, Sec. V summarizes the work and offers concluding remarks.

II. Problem Statement

Consider a body-fixed coordinate frame $\mathcal{F}_{\mathcal{B}}$ with origin at the center of mass of a rigid vehicle and coordinate vectors $\{\boldsymbol{x}_{\mathcal{B}}, \boldsymbol{y}_{\mathcal{B}}, \boldsymbol{z}_{\mathcal{B}}\}$. The vehicle's motion is assumed to be described in an inertial coordinate frame, $\mathcal{F}_{\mathcal{I}}$, with origin at the landing site and coordinate vectors $\{\boldsymbol{x}_{\mathcal{I}}, \boldsymbol{y}_{\mathcal{I}}, \boldsymbol{z}_{\mathcal{I}}\}$. Planetary rotation and any atmospheric effects are ignored for the study of optimal descent trajectories. We further assume a flat planet, so that the acceleration due to gravity is constant and $\boldsymbol{g}_{\mathcal{I}} = -g\boldsymbol{z}_{\mathcal{I}}$, where g is the acceleration due to gravity at the

Received 6 July 2019; revision received 14 November 2019; accepted for publication 5 March 2020; published online XX epubMonth XXXX.

*Ph.D. Candidate, Aeronautics and Astronautics; tpr@uw.edu. Student Member AIAA.

†Professor, Aeronautics and Astronautics; mesbahi@uw.edu. Associate Fellow AIAA.

‡A given translational trajectory dictates a set of orientations from which the landing site is visible to a fixed sensor boresight; conversely, for a given orientation, there is a set of positions that are acceptable in order to view the landing site.

surface of the planet under consideration. If the initial inertial position and velocity vectors lie in a plane that contains the landing site, then we may assume without loss of generality[§] that the vehicle's motion evolves in the $\boldsymbol{y}_{\mathcal{I}} - \boldsymbol{z}_{\mathcal{I}}$ plane. The inertial position and velocity vectors can then be written as $\boldsymbol{r}_{\mathcal{I}}(t) = [\, y(t) \;\; z(t) \,]^{\mathrm{T}} \in \mathbb{R}^2$ and $\boldsymbol{v}_{\mathcal{I}}(t) = [\, v_y(t) \;\; v_z(t) \,]^{\mathrm{T}} \in \mathbb{R}^2$, and the attitude of the vehicle can be represented by a single angle, which we denote by $\theta(t) \in \mathbb{R}$, and define to be the angle formed between $\boldsymbol{z}_{\mathcal{B}}$ and $\boldsymbol{z}_{\mathcal{I}}$.

We assume that a single main engine and separate torque-generating actuators provide the control authority during the descent. The main engine is assumed to be rigidly affixed to the vehicle so that the thrust direction is fixed in the body frame and passes through the center of mass. The main engine has a variable thrust magnitude denoted by $\Gamma(t) \in \mathbb{R}$. To control the attitude of the vehicle, a second torque input, $\tau(t) \in \mathbb{R}$ is assumed to be available that is independent from the body-fixed thrust. See Fig. 1 for an illustration of the control configuration.

The corresponding inertial thrust vector can be expressed as the product of the thrust magnitude and the (unit) direction vector that is a function of the vehicle's attitude:

$$\boldsymbol{u}_{\mathcal{I}}(t) = \Gamma(t)\boldsymbol{d}(t), \qquad \boldsymbol{d}(t) \coloneqq \begin{bmatrix} -\sin\theta(t) \\ \cos\theta(t) \end{bmatrix}. \tag{1}$$

The control variables are therefore the scalar-valued functions $\Gamma(\cdot)$ and $\tau(\cdot)$, each of which are assumed to be piecewise continuous. The equations of motion are given by

$$\dot{m}(t) = -\alpha\Gamma(t), \qquad \dot{\boldsymbol{r}}_{\mathcal{I}}(t) = \boldsymbol{v}_{\mathcal{I}}(t), \qquad \dot{\boldsymbol{v}}_{\mathcal{I}}(t) = \frac{\Gamma(t)}{m(t)}\boldsymbol{d}(t) + \boldsymbol{g}_{\mathcal{I}},$$
$$\dot{\theta}(t) = \omega(t), \qquad \dot{\omega}(t) = \frac{\tau(t)}{J}, \tag{2}$$

where α is the reciprocal of the effective exhaust velocity, $\omega(t) \in \mathbb{R}$ is the angular velocity, J is the (constant) inertia about the $\boldsymbol{x}_{\mathcal{B}}$ axis in the body frame. In previous work, we have studied the case of time-varying inertia and found that the optimal descent trajectories are insensitive to changes in J due to mass variations [23]. Both control inputs are assumed to be bounded according to

$$\Gamma_{\min} \le \Gamma(t) \le \Gamma_{\max}, \tag{3a}$$

$$-\tau_{\max} \le \tau(t) \le \tau_{\max}, \tag{3b}$$

where $\Gamma_{\min}, \Gamma_{\max}, \tau_{\max} \in \mathbb{R}_{++}$ are positive real numbers.

We constrain the initial and final states according to the following boundary conditions:

$$m(t_0) = m_{ic}, \quad \boldsymbol{r}_{\mathcal{I}}(t_0) = \boldsymbol{r}_{\mathcal{I},ic}, \quad \boldsymbol{v}_{\mathcal{I}}(t_0) = \boldsymbol{v}_{\mathcal{I},ic}, \quad \boldsymbol{\omega}_{\mathcal{B}}(t_0) = 0, \tag{4a}$$

$$\boldsymbol{r}_{\mathcal{I}}(t_f) = \boldsymbol{r}_{\mathcal{I},f}, \quad \boldsymbol{v}_{\mathcal{I}}(t_f) = \boldsymbol{v}_{\mathcal{I},f}, \quad \theta(t_f) = 0, \quad \boldsymbol{\omega}_{\mathcal{B}}(t_f) = 0. \tag{4b}$$

Note that the initial attitude is not constrained, a feature whose importance was discussed in [22] (section III.A.3) and plays an important role in the results of this work as well.

The minimum-fuel planar powered descent guidance problem is summarized in Problem 1. Given an initial time $t_0 \in \mathbb{R}_+$, we wish to find the final time, $t_f \in \mathbb{R}_{++}$ and the piecewise continuous inputs $\Gamma(t)$, $\tau(t)$ for $t \in [t_0, t_f]$ that solve the following optimal control problem:

Problem 1:

$$\min_{t_f, \Gamma(\cdot), \tau(\cdot)} \quad \int_{t_0}^{t_f} \Gamma(t)\, \mathrm{d}t$$
$$\text{subject to:} \quad (2),\ (3),\ (4).$$

[§]This is provided that there are no state constraints that couple the rotational and translational motion; see Ref. [22] for an example where out-of-plane motion can be induced by such a constraint.

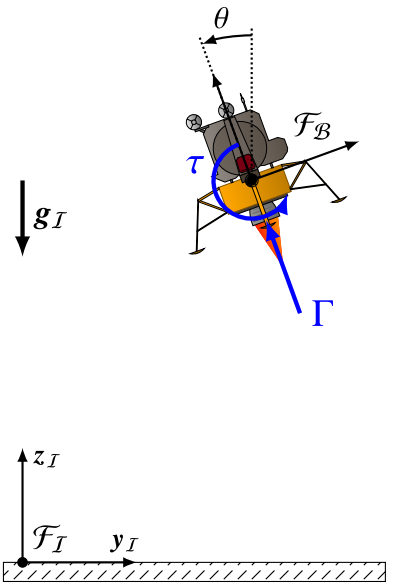

Fig. 1 Illustration of the planar landing scenario considered in this paper.

III. Solution to the Optimal Planar Powered Descent Problem

This section describes the optimal solutions to Problem 1. The necessary conditions of optimality are obtained from the maximum principle [27–29], and the specific version that is used is provided as Theorem III.1. We define the state vector $\boldsymbol{x}(t) = [\, m(t) \;\; \boldsymbol{r}_{\mathcal{I}}(t)^{\mathrm{T}} \;\; \boldsymbol{v}_{\mathcal{I}}(t)^{\mathrm{T}} \;\; \theta(t) \;\; \omega(t) \,]^{\mathrm{T}} \in \mathbb{R}^n$ and control vector $\boldsymbol{u}(t) = [\, \Gamma(t) \;\; \tau(t) \,]^{\mathrm{T}} \in \mathbb{R}^m$, where $n = 7$ and $m = 2$. The dynamics in (2) can then be written in the form $\dot{\boldsymbol{x}}(t) = f(\boldsymbol{x}(t), \boldsymbol{u}(t))$ for a suitably defined function f. The set of feasible controls given by (3) is denoted by $\mathcal{U} \subset \mathbb{R}^m$. Let the set $\mathcal{B} \coloneqq \{(\boldsymbol{x}(t_0), t_0, \boldsymbol{x}(t_f), t_f) | t_0 = 0, \text{(4a) and (4b) are satisfied}\}$ describe the set of admissible endpoints for Problem 1. Next, define the Hamiltonian $\mathcal{H} : \mathbb{R}^{2n+m+1} \to \mathbb{R}$ as

$$\mathcal{H}(\boldsymbol{x}(t), \boldsymbol{u}(t), \boldsymbol{\lambda}(t), \lambda^0) \coloneqq \lambda^0 L(\boldsymbol{u}(t)) + \boldsymbol{\lambda}(t)^{\mathrm{T}} f(\boldsymbol{x}(t), \boldsymbol{u}(t)), \tag{5}$$

where $L(\cdot)$ is the running cost of Problem 1, and $(\lambda^0, \boldsymbol{\lambda}(t)) \in \mathbb{R}^{n+1}$ is the costate vector. The (nonlinear) function f is assumed to be at least once continuously differentiable with respect to $\boldsymbol{x}$ (that is, we assume that $m(t) > 0$) and both f and L are assumed to be continuous functions of $\boldsymbol{u}$. Finally, we define $\pi(t) \coloneqq (\boldsymbol{x}^*(t), \boldsymbol{u}^*(t), \boldsymbol{\lambda}^*(t), \lambda^{0*})$, where the superscript * denotes an optimal quantity.

Theorem III.1 (maximum principle): Let t_f^* denote the optimal final time, and $\boldsymbol{u}^* : [t_0, t_f^*] \to \mathcal{U}$ an optimal control with corresponding state $\boldsymbol{x}^* : [t_0, t_f^*] \to \mathbb{R}^n$. Then the following statements hold:

1) There exists an absolutely continuous function $\boldsymbol{\lambda}^* : [t_0, t_f^*] \to \mathbb{R}^n$ and a constant $\lambda^{0*} \le 0$ such that $(\lambda^{0*}, \boldsymbol{\lambda}^*(t)) \neq 0$ for almost all $t \in [t_0, t_f^*]$.

2) The following canonical equations hold:

$$\dot{\boldsymbol{x}}^*(t) = \mathcal{H}_{\lambda}(\pi(t)), \tag{6a}$$

$$\dot{\boldsymbol{\lambda}}^*(t) = -\mathcal{H}_{x}(\pi(t)). \tag{6b}$$

3) For $t \in [t_0, t_f^*]$, the pointwise maximization criterion holds almost everywhere:

$$\mathcal{H}(\pi(t)) = \max_{\boldsymbol{w}(t) \in \mathcal{U}} \mathcal{H}(\boldsymbol{x}^*(t), \boldsymbol{w}(t), \boldsymbol{\lambda}^*(t), \lambda^{0*}). \tag{7}$$

4) The $(2n + 2)$-vector

$$[\mathcal{H}(\pi(t_0)), -\boldsymbol{\lambda}^*(t_0), -\mathcal{H}(\pi(t_f^*)), \boldsymbol{\lambda}^*(t_f^*)] \tag{8}$$

is orthogonal to the tangent space of $\mathcal{B}$ at the point $(t_0, \boldsymbol{x}^*(t_0), t_f^*, \boldsymbol{x}^*(t_f^*))$.

A. Existence of Optimal Solutions to Problem 1

Let us first establish the existence of optimal solutions to Problem 1. Suppose that there exists a feasible solution to Problem 1. Let $\mathcal{I} \subset \mathbb{R}$ be a compact interval and $\mathcal{X} \subset \mathbb{R}^n$ and $\mathcal{V} \in \mathbb{R}^m$ be suitably defined open regions such that any feasible solution satisfies $\boldsymbol{x}(t) \in \mathcal{X}$ and $\boldsymbol{u}(t) \in \mathcal{V}$. The composite function $(L, f) : \mathcal{I} \times \mathcal{X} \times \mathcal{V} \to \mathbb{R}^{n+1}$ defined by the cost function in Problem 1 and the dynamics given in (2) is continuous for the planar landing problem. Furthermore, by assuming that the initial attitude satisfies $\theta(t_0) \in [-\pi, \pi]$, the final time is bounded by some $t_{f,\max}$, and the final mass satisfies $m(t_f) > 0$,[¶] the set of admissible endpoints $\mathcal{B}$ is a closed set of points in $\mathbb{R}^{2n+2}$ and we may say that $[t_0 \ \boldsymbol{x}(t_0)^\top]^\top \in \mathcal{I} \times \mathcal{X}$ and $[t_f \ \boldsymbol{x}(t_f)^\top]^\top \in \mathcal{I} \times \mathcal{X}$. The set of admissible controls $\mathcal{U}$ is a compact and convex subset of $\mathcal{V}$ since it is defined by (3). Since the dynamics are affine in control and $\mathcal{U}$ is convex, there exists a compact set $\mathcal{R} \subset \mathcal{I} \times \mathcal{X}$ such that all feasible trajectories are contained in $\mathcal{R}$. This follows from Filippov's theorem [29]. Based on these observations, if the set

$$\mathcal{Q}^+(t, \boldsymbol{x}) = \{\hat{\boldsymbol{y}} = (y^0, \boldsymbol{y}) | y^0 \geq L(\boldsymbol{w}), \boldsymbol{y} = f(\boldsymbol{x}, \boldsymbol{w}), \boldsymbol{w} \in \mathcal{U}\} \quad (9)$$

is convex, then by theorem 4.4.2 of Ref. [30], an optimal solution to Problem 1 exists. A vector $(y^0, \boldsymbol{y}) \in \mathcal{Q}^+(t, \boldsymbol{x})$—where $\boldsymbol{y} = [y_1 \ \ \boldsymbol{y}_2^\top \ \ \boldsymbol{y}_3^\top \ \ y_4 \ \ y_5]^\top$ for $y_1, y_4, y_5 \in \mathbb{R}$ and $\boldsymbol{y}_2, \boldsymbol{y}_3 \in \mathbb{R}^2$—if and only if

$$y^0 \geq w_1, \quad y_1 = -\alpha w_1, \quad \boldsymbol{y}_2 = \boldsymbol{v}_{\mathcal{I}}, \quad \boldsymbol{y}_3 = \frac{w_1}{m}\boldsymbol{d} + \boldsymbol{g}_{\mathcal{I}}, \quad (10a)$$

$$y_4 = \omega, \ \ y_5 = \frac{w_2}{J}, \ \ \Gamma_{\min} \leq w_1 \leq \Gamma_{\max}, \ \ -\tau_{\max} \leq w_2 \leq \tau_{\max}. \quad (10b)$$

These constitute a set of linear equalities and inequalities, and hence the set $\mathcal{Q}^+(t, \boldsymbol{x})$ is convex. As such, an optimal solution to Problem 1 exists, provided that a feasible one does.

B. Optimal Solutions for Problem 1

To simplify notation, we will suppress the argument of time and superscript * in this section unless they are explicitly needed. The Hamiltonian associated with Problem 1 is

$$\mathcal{H} = \lambda^0\Gamma - \lambda_m\alpha\Gamma + \boldsymbol{\lambda}_r^\top\boldsymbol{v} + \boldsymbol{\lambda}_v^\top\left(\frac{\Gamma}{m}\boldsymbol{d} + \boldsymbol{g}_{\mathcal{I}}\right) + \lambda_\theta\boldsymbol{\omega}_{\mathcal{B}} + \lambda_\omega\frac{\tau}{J}, \quad (11)$$

where $\lambda^0 \leq 0$ and $\boldsymbol{\lambda} \coloneqq [\lambda_m \ \boldsymbol{\lambda}_r^\top \ \boldsymbol{\lambda}_v^\top \lambda_\theta \ \lambda_\omega]^\top \in \mathbb{R}^7$. From (6b), the following equations govern the evolution of the optimal costate vector,

$$\dot{\lambda}_m = \frac{\Gamma}{m^2}\boldsymbol{\lambda}_v^\top\boldsymbol{d}, \ \ \dot{\boldsymbol{\lambda}}_r = 0, \ \ \dot{\boldsymbol{\lambda}}_v = -\boldsymbol{\lambda}_r, \ \ \dot{\lambda}_\theta = -\frac{\Gamma}{m}\boldsymbol{\lambda}_v^\top\boldsymbol{d}_\theta, \ \ \dot{\lambda}_\omega = -\lambda_\theta, \quad (12)$$

where $\boldsymbol{d}_\theta = [-\cos\theta \ -\sin\theta]^\top$ is the derivative of $\boldsymbol{d}$ with respect to θ. The transversality conditions derived from Theorem III.1.4 are

$$\mathcal{H}(\pi(t_f)) = 0, \qquad \lambda_\theta(t_0) = 0, \qquad \lambda_m(t_f) = 0. \quad (13)$$

The vector $\boldsymbol{\lambda}_v$ is typically referred to as the *primer vector* for the 3-DOF problem, and provides the optimal thrust direction for that problem [2]. A key intuitive observation is that when $\tau_{\max} \to \infty$, the translational components of the optimal planar solution approach the optimal 3-DOF solution. This can be seen by noting that $\boldsymbol{d}$ can be made arbitrarily close to $\boldsymbol{\lambda}_v/\|\boldsymbol{\lambda}_v\|_2$ given an infinite control authority via the input τ. The desire to point $\boldsymbol{d}$ in this direction follows from the integral form of the maximum principle given in [28]. However, limitations on τ and boundary conditions on the attitude variables render the solutions to the 3-DOF and planar problems distinct in general. This is because the unit direction $\boldsymbol{\lambda}_v/\|\boldsymbol{\lambda}_v\|_2$ may not be consistent with the attitude boundary conditions and/or changes too rapidly for the attitude control system to follow by using the bounded torque input. We might still expect, however, that in the presence of a constrained control input τ, the primer vector will be tracked when possible. This intuition is formalized in the remainder of this section.

Importantly, we can see that the costate expressions for $\boldsymbol{\lambda}_r$ and $\boldsymbol{\lambda}_v$ in (12) match those known to occur for the 3-DOF problem [2,31]. Namely, their solutions are

$$\boldsymbol{\lambda}_r(t) = \boldsymbol{c}_r, \quad \text{and} \quad \boldsymbol{\lambda}_v(t) = -\boldsymbol{c}_r t + \boldsymbol{c}_v, \quad (14)$$

where $\boldsymbol{c}_r, \boldsymbol{c}_v \in \mathbb{R}^2$ are constant vector quantities. Note that these vectors do not have the same numerical value between the 3-DOF problem and a planar landing problem; only the analytic expressions match. For future reference, we define the switching functions associated with the thrust and torque as follows:

$$\mathcal{H}_\Gamma \coloneqq \frac{1}{m}\boldsymbol{\lambda}_v^\top\boldsymbol{d} - \alpha\lambda_m + \lambda^0, \quad (15a)$$

$$\mathcal{H}_\tau \coloneqq \frac{1}{J}\lambda_\omega. \quad (15b)$$

We first establish the fact that the costate vector corresponding to the velocity is non-zero almost everywhere along an optimal trajectory. This preliminary result is key to the following analysis.

Lemma III.2: The vector $\boldsymbol{\lambda}_v(t)$ is non-zero for almost all $t \in [t_0, t_f]$.

Proof: The proof is by contradiction. Suppose that $\boldsymbol{\lambda}_v(t) = 0$ for some interval $t \in [t_1, t_2]$, where $t_0 \leq t_1 < t_2 \leq t_f$. Then, (14) implies that $\boldsymbol{\lambda}_v(t) = 0$ and $\boldsymbol{\lambda}_r(t) = 0$ for all $t \in [t_0, t_f]$. By virtue of the second and third transversality conditions in (13) and the corresponding costate dynamics in (12), we then have that $\lambda_m(t) = 0$ and $\lambda_\theta(t) = 0$ for all $t \in [t_0, t_f]$. Hence $\lambda_\omega(t) = c_\omega$ for some constant $c_\omega \in \mathbb{R}$. The transversality condition $\mathcal{H}(\pi(t_f)) = 0$ then leads to $\lambda^0 = -c_\omega\tau/J\Gamma$. If c_ω is zero, then $\lambda^0 = 0$ and Theorem III.1.1 is violated, so $c_\omega \neq 0$. The switching function $\mathcal{H}_\tau$ in this case implies that the optimal torque is then $\tau = \text{sign}(c_\omega)\tau_{\max} = \pm\tau_{\max}$ for all $t \in [t_0, t_f]$. The dynamic equation governing the angular velocity from (2) then leads to

$$\boldsymbol{\omega}_{\mathcal{B}}(t_f) - \boldsymbol{\omega}_{\mathcal{B}}(t_0) = \int_{t_0}^{t_f}\dot{\omega}_{\mathcal{B}}\,\mathrm{d}t = \pm\int_{t_0}^{t_f}\frac{\tau_{\max}}{J}\,\mathrm{d}t \neq 0, \quad (16)$$

which contradicts the boundary conditions $\boldsymbol{\omega}_{\mathcal{B}}(t_f) = \boldsymbol{\omega}_{\mathcal{B}}(t_0) = 0$ assumed in (4). Hence we cannot have $\boldsymbol{\lambda}_v(t) = 0$ along an optimal trajectory. □

The following theorem provides one of the main results of this paper.

Theorem III.3: The thrust magnitude is non-singular almost everywhere along an optimal solution of Problem 1.

Proof: The proof is performed in two steps, first by assuming that the torque input is singular, and then by assuming that it is non-singular. If the torque is singular for some interval of time $t \in [t_1, t_2]$, where $t_0 \leq t_1 < t_2 \leq t_f$, then the Hamiltonian reveals that we must have $\lambda_\omega = 0$ for all $t \in [t_1, t_2]$. On this same time interval we must then have $\dot{\lambda}_\omega = 0$ and hence $\lambda_\theta = \dot{\lambda}_\theta = 0$. Using the costate equations in (12) this implies that $0 = \boldsymbol{\lambda}_v^\top\boldsymbol{d}_\theta$ since Γ and m are strictly positive. This tells us that the vector $\boldsymbol{\lambda}_v$ is orthogonal to $\boldsymbol{d}_\theta$ for all times when the torque is singular. Since $\boldsymbol{d}$ and $\boldsymbol{d}_\theta$ are also orthogonal, we conclude that $\boldsymbol{d}$ and $\boldsymbol{\lambda}_v$ must be either parallel or anti-parallel. The switching function associated with the thrust magnitude is

$$\mathcal{H}_\Gamma = \frac{1}{m}\boldsymbol{\lambda}_v^\top\boldsymbol{d} - \alpha\lambda_m + \lambda^0. \quad (17)$$

[¶]Similar to Ref. [10], the limited fuel carried by the vehicle naturally leads to the existence of a $t_{f,\max}$ and non-zero lower bound on $m(t_f)$.

For $t \in [t_1, t_2]$ we then have

$$\dot{\mathcal{H}}_\Gamma = \frac{\alpha\Gamma}{m^2}\boldsymbol{\lambda}_v^\top \boldsymbol{d} - \frac{1}{m}\boldsymbol{\lambda}_r^\top \boldsymbol{d} + \frac{\omega}{m}\boldsymbol{\lambda}_v^\top \boldsymbol{d}_\theta - \frac{\alpha\Gamma}{m^2}\boldsymbol{\lambda}_v^\top \boldsymbol{d}, \tag{18a}$$

$$= -\frac{1}{m}\boldsymbol{\lambda}_r^\top \boldsymbol{d}, \tag{18b}$$

since $\boldsymbol{\lambda}_v^\top \boldsymbol{d}_\theta = 0$. Note that if $\boldsymbol{\lambda}_r^\top \boldsymbol{d} = 0$, then by virtue of $\boldsymbol{d} = \pm\boldsymbol{\lambda}_v/\|\boldsymbol{\lambda}_v\|_2$ we know that $\boldsymbol{\lambda}_r^\top \boldsymbol{\lambda}_v = 0$. From (14) this implies that $-\|\boldsymbol{c}_r\|_2^2 t + \boldsymbol{c}_r^\top \boldsymbol{c}_v = 0$ for all $t \in [t_1, t_2]$. From Lemma III.2 we cannot have both $\boldsymbol{c}_r$ and $\boldsymbol{c}_v$ zero, and thus it must be that $\boldsymbol{\lambda}_r(t) = \boldsymbol{c}_r = 0$. Hence $\dot{\mathcal{H}}_\Gamma = 0$ only if $\boldsymbol{\lambda}_r = 0$ on the interval $[t_1, t_2]$. We can show that $\mathcal{H}_\Gamma \neq 0$ when $\boldsymbol{\lambda}_r = 0$ to complete the proof, since even if $\dot{\mathcal{H}} = 0$ we will have established that a singular arc is not possible. Assume for a contradiction that $\boldsymbol{\lambda}_r = 0$ and $\mathcal{H}_\Gamma = 0$ for $t \in [t_1, t_2]$. Using the transversality condition $\mathcal{H}(\pi(t_f)) = 0$, it follows that $\mathcal{H}(\pi(t_f)) = \boldsymbol{\lambda}_v^\top \boldsymbol{g}_\mathcal{I} = 0$. Because $\boldsymbol{\lambda}_v$ and $\boldsymbol{d}$ are either parallel or anti-parallel, this implies that $\boldsymbol{d}^\top \boldsymbol{g}_\mathcal{I} = 0$. However this condition says that the attitude is orthogonal to the gravity vector, which means that there is no ability to thrust in the vertical direction, and hence the vehicle is in vertical freefall. This contradicts a wide variety of common boundary conditions. Hence, $\mathcal{H}_\Gamma \neq 0$ almost everywhere when $t \in [t_1, t_2]$ if $\boldsymbol{\lambda}_r = 0$. As a result, the thrust must be non-singular.

Assume now that the torque is non-singular, so that $\tau = \pm\tau_{\max}$, for some interval of time $t \in [t_1, t_2]$, where $t_0 \leq t_1 < t_2 \leq t_f$. In this case, one may directly solve the attitude state equations on this interval to yield

$$\theta(t) = \theta(t_1) + \omega(t_1)(t - t_1) \pm \frac{1}{2}\frac{\tau_{\max}}{J}(t - t_1)^2, \quad \forall\, t \in [t_1, t_2]. \tag{19}$$

The switching function for the thrust magnitude is still given by $\mathcal{H}_\Gamma$ in (17). If the thrust is singular, then $\mathcal{H}_\Gamma = 0$ for all $t \in [t_1, t_2]$. Accordingly, we would have $\dot{\mathcal{H}}_\Gamma = 0$ for $t \in [t_1, t_2]$. Using (18a) this implies that

$$\dot{\mathcal{H}}_\Gamma = -\frac{1}{m}\boldsymbol{\lambda}_r^\top \boldsymbol{d} + \frac{\omega}{m}\boldsymbol{\lambda}_v^\top \boldsymbol{d}_\theta \tag{20a}$$

$$0 = \frac{1}{m}\frac{\mathrm{d}}{\mathrm{d}t}(\boldsymbol{\lambda}_v^\top \boldsymbol{d}), \tag{20b}$$

which implies that $\boldsymbol{\lambda}_v^\top \boldsymbol{d}$ is constant. However, since we know the form of $\boldsymbol{\lambda}_v$ as an explicit function of time via (14), we can combine this with (19) to obtain $\boldsymbol{\lambda}_v^\top \boldsymbol{d}$ as an explicit function of time. The resulting function can be neither zero nor constant over an interval of time. Essentially, the vector $\boldsymbol{\lambda}_v$ varies as a linear function of time, whereas the vector $\boldsymbol{d}$ varies sinusoidally with a frequency that increases quadratically in time. They cannot be perpendicular for an interval of time, but rather only at finitely many instants of time between t_1 and t_2. This implies that $\dot{\mathcal{H}}_\Gamma \neq 0$ for almost all $t \in [t_1, t_2]$. As a result, $\mathcal{H}_\Gamma = 0$ is not possible except at a finite number of instants over the interval $[t_1, t_2]$. Hence, the thrust magnitude is non-singular almost everywhere on this interval. □

Theorem III.3 shows that the thrust magnitude must always be non-singular for an optimal solution, regardless of the value of the torque input. Since singular torque arcs may occur, we now characterize what these singular torques can look like. The switching function for the torque input is given by

$$\mathcal{H}_\tau = \frac{1}{J}\lambda_\omega. \tag{21}$$

Along a torque-singular arc, we have $\mathcal{H}_\tau = 0$. Taking Lie derivatives along extremal solutions results in

$$J\mathcal{H}_\tau^{(1)} = -\lambda_\theta, \tag{22a}$$

$$J\mathcal{H}_\tau^{(2)} = \frac{\Gamma}{m}\boldsymbol{\lambda}_v^\top \boldsymbol{d}_\theta, \tag{22b}$$

$$J\mathcal{H}_\tau^{(3)} = \frac{\alpha\Gamma^2}{m^2}\boldsymbol{\lambda}_v^\top \boldsymbol{d}_\theta - \frac{\Gamma}{m}\boldsymbol{\lambda}_r^\top \boldsymbol{d}_\theta - \frac{\Gamma\omega}{m}\boldsymbol{\lambda}_v^\top \boldsymbol{d}, \tag{22c}$$

$$J\mathcal{H}_\tau^{(4)} = \left(\frac{\alpha^2\Gamma^3}{m^3} - \frac{\Gamma\omega^2}{m^2}\right)\boldsymbol{\lambda}_v^\top \boldsymbol{d}_\theta - \frac{2\alpha\Gamma^2}{m^2}\boldsymbol{\lambda}_r^\top \boldsymbol{d}_\theta + \frac{2\Gamma\omega}{m}\boldsymbol{\lambda}_r^\top \boldsymbol{d} - \left(\frac{2\alpha\Gamma^2\omega}{m^2} + \frac{\Gamma}{mJ}\tau\right)\boldsymbol{\lambda}_v^\top \boldsymbol{d}, \tag{22d}$$

each of which must be zero along torque-singular arcs. The singular arc is therefore *second-order*. As is already known from the proof of Theorem III.3 the condition (22b) reveals that $\boldsymbol{\lambda}_v^\top \boldsymbol{d}_\theta = 0$. Substituting this into (22c) yields

$$\boldsymbol{\lambda}_r^\top \boldsymbol{d}_\theta = -\omega\boldsymbol{\lambda}_v^\top \boldsymbol{d}, \tag{23}$$

along torque-singular arcs. Using (22b) and (23) in (22d) then leads to

$$\tau = 2J\omega\frac{\boldsymbol{\lambda}_r^\top \boldsymbol{d}}{\boldsymbol{\lambda}_v^\top \boldsymbol{d}}. \tag{24}$$

The generalized (Legendre–Clebsch) convexity condition further reveals that

$$\frac{1}{J}\boldsymbol{\lambda}_v^\top \boldsymbol{d} \geq 0, \tag{25}$$

which, in addition to the fact that $\boldsymbol{\lambda}_v^\top \boldsymbol{d}_\theta = 0$, implies that $\boldsymbol{d} = \hat{\boldsymbol{\lambda}}_v \coloneqq \boldsymbol{\lambda}_v/\|\boldsymbol{\lambda}_v\|_2$ along torque-singular arcs, confirming the intuition that the same behavior is observed as in the 3-DOF problem. We have shown here that this consistency is confined to times when the torque input is singular. This also shows that in cases where the torque is always singular, the most general thrust magnitude profile is max–min–max since the equations that govern the optimal planar solutions recover exactly those of the 3-DOF problem. However, it will not always be the case that $\boldsymbol{d} = \hat{\boldsymbol{\lambda}}_v$ for an entire planar landing trajectory due to boundary conditions on the vehicle attitude, vehicle characteristics (e.g., inertia) and torque limitations. The following result establishes the switching structure of the optimal thrust input for planar landing problems.

Lemma III.4: The most general switching structure for the optimal thrust input of a planar landing problem is min–max–min–max–min.

Proof: Note that when $\boldsymbol{d} = \hat{\boldsymbol{\lambda}}_v$ the most general switching structure is max–min–max, inherited from the 3-DOF solution as proven above. To establish the result, we explore how minimum thrust arcs are possible at the beginning and end of a trajectory. For cases where $\boldsymbol{d} \neq \hat{\boldsymbol{\lambda}}_v$ at the initial time, the torque input will be used to steer the attitude towards $\boldsymbol{d} = \hat{\boldsymbol{\lambda}}_v$. According to the integral form of the maximum principle [28], this ought to happen as quickly as possible, resulting in a non-singular torque arc. Hence, the value of the inner product $\boldsymbol{\lambda}_v^\top \boldsymbol{d}$ will be *increasing* during this time, implying that its time derivative is positive. If the torque is non-singular, the sign of (20b) implies that a switch from minimum thrust to maximum thrust is possible. When the initial attitude is free, as in Problem 1, we can expect that this case would arise infrequently; the optimal solution will be chosen so that its initial attitude satisfies $\boldsymbol{d} = \hat{\boldsymbol{\lambda}}_v$. A constrained initial attitude could therefore induce an initial minimum thrust arc.

On the other hand, the terminal attitude boundary condition may impose that $\boldsymbol{d} \neq \hat{\boldsymbol{\lambda}}_v$ at the final time. It is therefore possible that the inner product $\boldsymbol{\lambda}_v^\top \boldsymbol{d}$ *decreases* in value at the end of the trajectory. Hence the sign of (20b) implies that a switch from maximum to minimum thrust is possible at the end of the trajectory if the torque is again non-singular during this period. □

The presence of an initial or terminal minimum thrust arc is governed by the boundary conditions and control constraints of the

Table 1 Problem parameters for the planar landing example

Parameter	Value	Units
m_{ic}	2.0	Mass unit (MU)
α	0.0034	Time unit/length unit (TU/LU)
$\boldsymbol{r}_{\mathcal{I},ic}$	$[4.5\ \ 16.5]^\mathsf{T}$	LU
$\boldsymbol{r}_{\mathcal{I},f}$	$[0\ \ 0]^\mathsf{T}$	LU
$\boldsymbol{v}_{\mathcal{I},ic}$	$[-10.0\ \ -1.5]^\mathsf{T}$	LU/TU
$\boldsymbol{v}_{\mathcal{I},f}$	$[0\ \ 0]^\mathsf{T}$	LU/TU
ω_{ic}	0	rad/TU
ω_f	0	rad/TU
θ_f	0	rad
g	-1	LU/TU^2
$\Gamma_{\min}$	1.5	Force unit (FU)
$\Gamma_{\max}$	6.5	FU
$\tau_{\max}$	1	FU LU
J	0.25	MU LU^2

problem, as well as the physical vehicle parameters. Of course, we note that simply constraining the attitude at either endpoint does not *guarantee* the presence of a minimum thrust arc, but does represent a necessary condition. This is explored in more detail in Sec. IV.

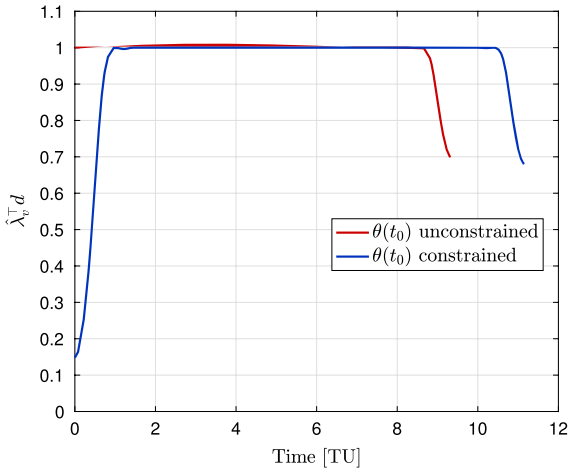

Fig. 4 Inner product between the thrust direction d and $\hat{\lambda}_v \equiv \lambda_v / \|\lambda_v\|_2$ along optimal solutions to planar landing problems.

IV. Numerical Solutions

An example planar landing scenario is now presented whose optimal solution showcases the characteristics derived in Sec. III. All numerical results are obtained using GPOPS-II [32], and the problem parameters are given in Table 1. To highlight the switching structure of this problem, the boundary conditions were

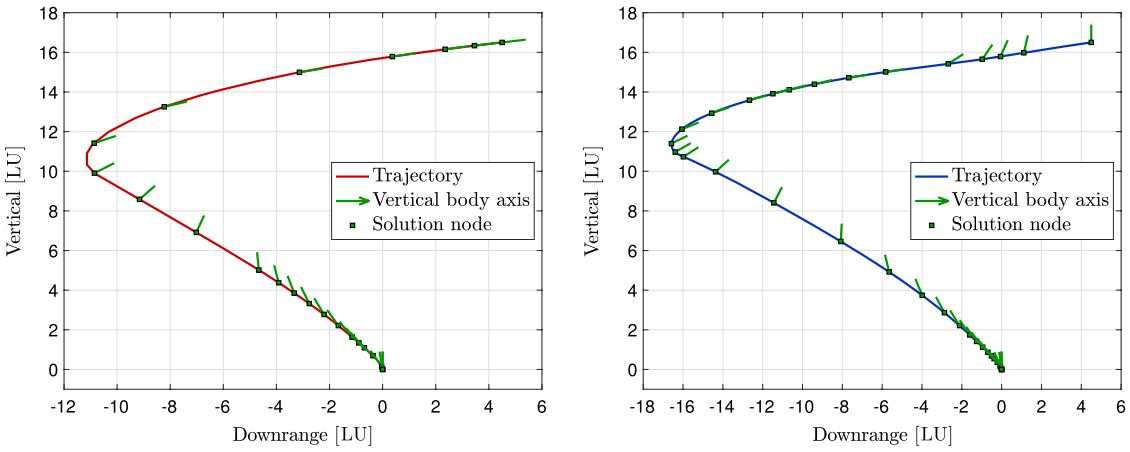

a) Initial attitude $\theta(t_0)$ unconstrained **b) Initial attitude $\theta(t_0)$ constrained**

Fig. 2 Optimal trajectories for the planar landing problems. Only one-quarter of the solution nodes are shown for clarity.

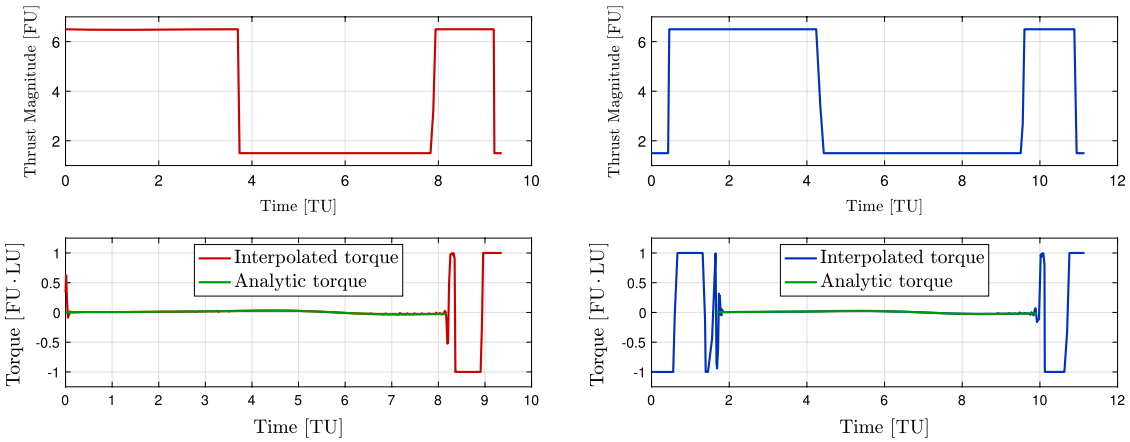

a) Initial attitude $\theta(t_0)$ unconstrained **b) Initial attitude $\theta(t_0)$ constrained**

Fig. 3 Optimal inputs for the planar landing problems.

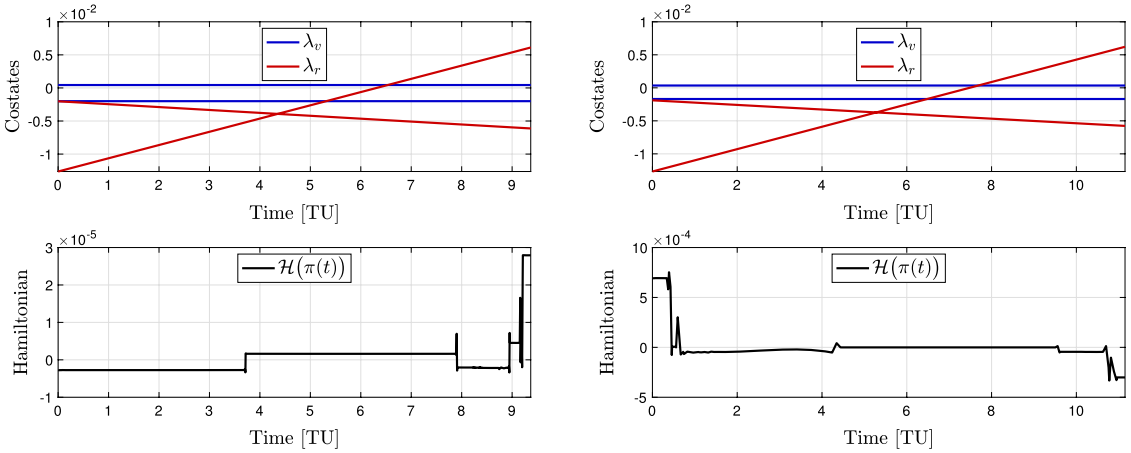

a) Initial attitude $\theta(t_0)$ unconstrained **b) Initial attitude $\theta(t_0)$ constrained**

Fig. 5 Select costates and the Hamiltonian for the planar landing problems.

selected so that a minimum thrust arc was observed at the end of the trajectory. By re-solving the same problem a second time with the initial attitude constrained, we are further able to introduce an initial minimum thrust arc, thus providing an example that highlights the min–max–min–max–min switching structure and supports the observation that the presence of an initial attitude constraint can induce an initial minimum thrust arc (since $\boldsymbol{d} \neq \hat{\boldsymbol{\lambda}}_v$).

The optimal planar trajectories are given in Fig. 2, where the thrust is always directed along the vertical body axis depicted by the green lines. The corresponding optimal inputs are given in Fig. 3. When the initial attitude is unconstrained, it is selected to be in the direction of $\hat{\boldsymbol{\lambda}}_v$, as shown by Fig. 4. Accordingly, no minimum thrust arc is observed at the beginning of the maneuver. By constraining the initial attitude, Fig. 4 confirms that $\boldsymbol{d} \neq \hat{\boldsymbol{\lambda}}_v$ near the beginning of the maneuver, and since the torque is non-singular, a minimum thrust arc can be seen at the initial time in Fig. 3. In both cases, due to the boundary condition imposed at the final time that $\theta(t_f) = 0$, it follows that $\boldsymbol{d} \neq \hat{\boldsymbol{\lambda}}_v$ near the end of the maneuver. Since the torque is non-singular, a minimum thrust arc is observed at the final time in each graph of Fig. 3. The optimality of these trajectories is verified by Fig. 5, where key necessary conditions derived in Sec. III are plotted against time. In each case the values of $\lambda_m(t_f)$ and $\lambda_\theta(t_0)$ (when appropriate) were verified to be less than 10^{-8}.

The torque input in either case can be seen to saturate near the endpoints for which an attitude constraint is enforced. This would imply that the primer vector is tracked for as much of the planar landing solution as possible, with rotational maneuvers occurring as fast as is feasible whenever the satisfaction of a boundary condition is required. This observation follows naturally from the integral form of the maximum principle [28], whereby the pointwise maximization criterion of Theorem III.1.3 is replaced by its integral over $[t_0, t_f]$, revealing the need to have $\boldsymbol{d} = \hat{\boldsymbol{\lambda}}_v$ for as much of the trajectory as possible.

A key difference between the two planar landing problems shown here and the 3-DOF problem is the optimal final time, t_f. For the 3-DOF problem, the optimal final time is 9.03 s for the parameters in Table 1. In contrast, the planar landing scenarios have optimal final times of 9.32 s when the initial attitude is unconstrained and 11.12 s when it is constrained. Different final times contribute in particular to different optimal $\boldsymbol{\lambda}_v$ for each problem, and hence different optimal state and control trajectories.**

The value of the analytic torque from (24) is shown alongside the numerical results in Fig. 3. These profiles are close to matching, but slight discrepancies may be caused by the fact that the GPOPS-II software can have difficulties obtaining solutions when singular arcs are present; and in particular, when they occur between non-singular arcs [32].

**Fixing the final time does not empirically cause the same values for $\boldsymbol{\lambda}_v$.

V. Conclusions

The planar landing problem for which there exists independent actuation mechanisms that are able to create bounded thrust and torque was studied. We showed that an optimal solution to this problem exists whenever a feasible solution does, and that the thrust magnitude must always lie at one of the bounds, while the torque may be singular along optimal solutions. Moreover, there can be up to four switches in the optimal thrust with a min–max–min–max–min profile. The minimum thrust arcs at the beginning and end of a trajectory are governed by the boundary conditions, torque limitations and physical vehicle parameters. These results provide new theoretical insights for a powered descent problem beyond the translation-only 3-DOF problem and offer a path towards the understanding of optimal 6-DOF powered descent problems.

Acknowledgments

This research has been supported by NASA grant NNX17AH02A and National Sciences and Engineering Research Council of Canada (NSERC) grant PGSD3-502758-2017. The authors would like to thank M. Szmuk, D. Malyuta, B. Açıkmeşe, and J. M. Carson, III, for many valuable discussions on the powered descent guidance problem.

References

[1] Klumpp, A. R., "Apollo Lunar-Descent Guidance," Charles Stark Draper Lab. Rept. R-695, 1971. https://doi.org/10.1016/0005-1098(74)90019-3

[2] Lawden, D., "Optimal Trajectories for Space Navigation," *Optimal Trajectories for Space Navigation*, Butterworths, London, 1963. https://doi.org/10.1016/0032-0633(64)90149-7

[3] Meditch, J. S., "On the Problem of Optimal Thrust Programming For a Lunar Soft Landing," *IEEE Transactions on Automatic Control*, Vol. 9, No. 4, 1964, pp. 477–484. https://doi.org/10.1109/TAC.1964.1105758

[4] Topcu, U., Casoliva, J., and Mease, K. D., "Minimum-Fuel Powered Descent for Mars Pinpoint Landing," *Journal of Spacecraft and Rockets*, Vol. 44, No. 2, 2007, pp. 324–331. https://doi.org/10.2514/1.25023

[5] D'Souza, C. N., "An Optimal Guidance Law for Planetary Landing," *AIAA Guidance, Navigation, and Control Conference*, AIAA Paper 1997-3709, 1997. https://doi.org/10.2514/6.1997-3709

[6] Lu, P., Forbes, S., and Baldwin, M., "A Versatile Powered Guidance Algorithm," *AIAA Guidance, Navigation, and Control Conference*, AIAA Paper 2012-4843, 2012. https://doi.org/10.2514/6.2012-4843

[7] Lu, P., "Propellant-Optimal Powered Descent Guidance," *Journal of Guidance, Control, and Dynamics*, Vol. 41, No. 4, 2018, pp. 813–826. https://doi.org/10.2514/1.G003243

[8] Najson, F., and Mease, K., "A Computationally Non-Expensive Guidance Algorithm for Fuel Efficient Soft Landing," *AIAA Guidance,*

Navigation, and Control Conference and Exhibit, AIAA Paper 2005-6289, 2005.
https://doi.org/10.2514/6.2005-6289

[9] Rea, J. R., and Bishop, R., "Analytical Dimensional Reduction of a Fuel Optimal Powered Descent Subproblem," *AIAA Guidance, Navigation, and Control Conference*, AIAA Paper 2010-8026, 2010.
https://doi.org/10.2514/6.2010-8026

[10] Açıkmeşe, B., and Ploen, S., "Convex Programming Approach to Powered Descent Guidance for Mars Landing," *Journal of Guidance, Control, and Dynamics*, Vol. 30, No. 5, 2007, pp. 1353–1366.
https://doi.org/10.2514/1.27553

[11] Açıkmeşe, B., , Carson, J. M., III, and Blackmore, L., "Lossless Convexification of Nonconvex Control Bound and Pointing Constraints of the Soft Landing Optimal Control Problem," *IEEE Transactions on Control Systems Technology*, Vol. 21, No. 6, 2013, pp. 2104–2113.
https://doi.org/10.1109/tcst.2012.2237346

[12] Carson, J. M., III, Açıkmeşe, B., Blackmore, L., and Wolf, A., "Capabilities of Convex Powered-Descent Guidance Algorithms for Pinpoint and Precision Landing," *IEEE Aerospace Conference*, IEEE, New York, 2011.
https://doi.org/10.1109/aero.2011.5747244

[13] Carson, J. M., III, Açıkmeşe, B., and Blackmore, L., "Lossless Convexification of Powered-Descent Guidance with Non-Convex Thrust Bound and Pointing Constraints," *IEEE American Control Conference*, IEEE, New York, 2011.
https://doi.org/10.1109/acc.2011.5990959

[14] Blackmore, L., Açıkmeşe, B., and Scharf, D. P., "Minimum-Landing-Error Powered-Descent Guidance for Mars Landing Using Convex Optimization," *Journal of Guidance, Control, and Dynamics*, Vol. 33, No. 4, 2010, pp. 1161–1171.
https://doi.org/10.2514/1.47202

[15] Dueri, D., Açıkmeşe, B., Scharf, D. P., and Harris, M. W., "Customized Real-Time Interior-Point Methods for Onboard Powered-Descent Guidance," *Journal of Guidance, Control, and Dynamics*, Vol. 40, No. 2, 2017, pp. 197–212.
https://doi.org/10.2514/1.G001480

[16] Scharf, D. P., Regehr, M. W., Vaughan, G. M., Benito, J., Ansari, H., Aung, M., Johnson, A., Casoliva, J., Mohan, S., and Dueri, D., et al., "ADAPT Demonstrations of Onboard Large-Divert Guidance with a VTVL Rocket," *IEEE Aerospace Conference*, IEEE, New York, 2014.
https://doi.org/10.1109/aero.2014.6836462

[17] Scharf, D. P., Açıkmeşe, B., Dueri, D., Benito, J., and Casoliva, J., "Implementation and Experimental Demonstration of Onboard Powered-Descent Guidance," *Journal of Guidance, Control, and Dynamics*, Vol. 40, No. 2, 2017, pp. 213–229.
https://doi.org/10.2514/1.G000399

[18] Carson, J. M., III, Munk, M. M., Sostaric, R. R., Estes, J. N., Amzajerdian, F., Blair, J. B., Rutishauser, D. K., Restrepo, C. I., Dwyer-Cianciolo, A., Chen, G. T., and Tse, T., "The SPLICE Project: Continuing NASA Development of GN&C Technologies for Safe and Precise Landing," *AIAA SciTech Forum*, AIAA Paper 2019-0660, 2019.
https://doi.org/10.2514/6.2019-0660

[19] Dwyer-Cianciolo, A. M., Striepe, S., Carson, J. M., III, Sostaric, R., Woffinden, D., Karlgaard, C. D., Lugo, R. A., Powell, R., and Tynis, J., "Defining Navigation Requirements for Future Missions," *AIAA SciTech Forum*, AIAA Paper 2019-0661, 2019.
https://doi.org/10.2514/6.2019-0661

[20] Lee, U., and Mesbahi, M., "Optimal Powered Descent Guidance with 6-DOF Line of Sight Constraints via Unit Dual Quaternions," *AIAA Guidance, Navigation, and Control Conference*, AIAA Paper 2015-0319, 2015.
https://doi.org/10.2514/6.2015-0319

[21] Lee, U., and Mesbahi, M., "Constrained Autonomous Precision Landing via Dual Quaternions and Model Predictive Control," *Journal of Guidance, Control, and Dynamics*, Vol. 40, No. 2, 2017, pp. 292–308.
https://doi.org/10.2514/1.G001879

[22] Reynolds, T. P., Szmuk, M., Malyuta, D., Mesbahi, M., Açıkmeşe, B., and Carson, J. M., III, "Dual Quaternion Based 6-DOF Powered Descent Guidance with State-Triggered Constraints," arXiv E-Prints, 2019, arXiv 1904.09248.

[23] Reynolds, T. P., Szmuk, M., Malyuta, D., Mesbahi, M., Açıkmeşe, B., and Carson, J. M., III, "A State-Triggered Line of Sight Constraint for 6-DOF Powered Descent Guidance Problems," *AIAA SciTech Forum*, AIAA Paper 2019-0924, 2019.
https://doi.org/10.2514/6.2019-0924

[24] Szmuk, M., Reynolds, T. P., Açıkmeşe, B., Mesbahi, M., and Carson, J. M., III, "Successive Convexification for Real-Time Rocket Landing Guidance with Compound State-Triggered Constraints," *AIAA SciTech Forum*, AIAA Paper 2019-0926, 2019.
https://doi.org/10.2514/6.2019-0926

[25] Szmuk, M., and Açıkmeşe, B., "Successive Convexification for 6-DOF Mars Rocket Powered Landing with Free-Final-Time," *AIAA Guidance, Navigation, and Control Conference*, AIAA Paper 2018-0617, 2018.
https://doi.org/10.2514/6.2018-0617

[26] Szmuk, M., Reynolds, T. P., and Açıkmeşe, B., "Successive Convexification for Real-Time 6-DOF Powered Descent Guidance with State-Triggered Constraints," arXiv E-Prints, 2018, arXiv 1811.10803.

[27] Pontryagin, L. S., Boltyanskii, V. G., Gamkrelidze, R. V., and Mishchenko, E. F., *The Mathematical Theory of Optimal Processes*, Gordon and Breach, New York, 1986.
https://doi.org/10.1201/9780203749319

[28] Berkovitz, L. D., *Optimal Control Theory*, Springer–Verlag, New York, 1974.
https://doi.org/10.1007/978-1-4757-6097-2

[29] Liberzon, D., *Calculus of Variations and Optimal Control Theory*, Princeton Univ. Press, Princeton, NJ, 2007.
https://doi.org/10.2307/j.ctvcm4g0s

[30] Berkovitz, L. D., and Medhin, N. G., *Nonlinear Optimal Control Theory*, CRC Press, Boca Raton, FL, 2013.
https://doi.org/10.1007/978-1-4757-6097-2

[31] Marec, J.-P., *Optimal Space Trajectories*, Elsevier Scientific Publishing, Amsterdam, 1979.
https://doi.org/10.1002/oca.4660040210

[32] Patterson, M. A., and Rao, A. V., "GPOPS-II: A MATLAB Software for Solving Multiple-Phase Optimal Control Problems Using hp-Adaptive Gaussian Quadrature Collocation Methods and Sparse Nonlinear Programming," *ACM Transactions on Mathematical Software*, Vol. 41, No. 1, 2014, pp. 1–37.
https://doi.org/10.1145/2684421